Insights into Photoinduced Electron Transfer between [Ru(bpy)(3)](2+) and [S2O8](2−) in Water: Computational and Experimental Studies

ARTICLE *in* THE JOURNAL OF PHYSICAL CHEMISTRY A · NOVEMBER 2009

Impact Factor: 2.69 · DOI: 10.1021/jp908409n · Source: PubMed

Insights into Photoinduced Electron Transfer between $[Ru(bpy)_3]^{2+}$ and $[S_2O_8]^{2-}$ in Water: Computational and Experimental Studies

Alexey L. Kaledin,* Zhuangqun Huang, Yurii V. Geletii, Tianquan Lian, Craig L. Hill, and Djamaladdin G. Musaev*

Cherry L. Emerson Center for Scientific Computation and Department of Chemistry, Emory University, Atlanta, Georgia 30322

Received: August 31, 2009; Revised Manuscript Received: October 1, 2009

We examine the mechanism of electron transfer between $[Ru(bpy)_3]^{2+}$ and $[S_2O_8]^{2-}$ in aqueous solutions using time-dependent density functional and transition charge density model levels of theory. The calculations support the existence of a short-lived, optically bright **S1** state that decays to lower-lying triplet states **T1** and **T2**. The **T1** state leads to the charge transfer products, that is, $[Ru(bpy)_3]^{3+} + SO_4^{-\bullet} + SO_4^{2-}$. It was shown that photoinduced (in the 420−520 nm wavelength range) electron transfer between $[Ru(bpy)_3]^{2+}$ and $[S_2O_8]^{2-}$ may proceed via both the "unimolecular" and "bimolecular" pathways, in agreement with the previous experimental findings. This distinction arises on the basis of a weak interaction between the two reactants. Analysis of excited electronic states and their spin−orbit mixing suggests that a photon excites a MLCT **S1** state of $[Ru(bpy)_3]^{2+}*/\{[Ru(bpy)_3]^{2+}\cdots[S_2O_8]^{2-}\}*$ that converts to the lower-lying **T2** state via spin−orbit interaction, which is an intermediate in the **S1** → **T2** → **T1** chain. Once the system has converted to **T1**, it can evolve toward charge transfer from $[Ru(bpy)_3]^{2+}*$ to $[S_2O_8]^{2-}$ via elongation of the peroxo O−O bond that brings the "zero order" states of the $[Ru(bpy)_3]^{2+}*$ and $[S_2O_8]^{2-}$ fragments into (near) resonance. An exciton interaction model in combination with the transition charge density model provides excellent agreement with TD-DFT and allows us to obtain insight into the electron transfer process. The steady-state luminescence studies of the quenching of $[Ru(bpy)_3]^{2+}*$ in aqueous solutions by $[S_2O_8]^{2-}$ at pH 7.2 and 20 mM sodium phosphate buffer, the exact conditions used in our previous study of water oxidation [Geletii, Y. V.; Huang, Z. Q.; Hou, Y.; Musaev, D. G.; Lian, T. Q.; Hill, C. L. *J. Am. Chem. Soc.* **2009**, *131*, 7522−7523], show that 61% of the $[Ru(bpy)_3]^{2+}$ forms a ground state ion-pair complex $[Ru(bpy)_3]^{2+}\cdots[S_2O_8]^{2-}$, and the unimolecular ET rate is 2.5 times faster than for the bimolecular process. The concentration of the ion-pair complexes decreases at higher sodium phosphate buffer.

1. Introduction

The direct, efficient, sustained, sunlight-driven splitting of water into H_2 and O_2, one of the grand technical challenges, requires an O_2 evolution catalyst (water oxidation catalyst, or WOC), visible light photosensitizer, and H_2 evolution catalyst (HEC). Recently, we[1] and others[2] reported the efficient sustained oxidation of H_2O by $[Ru(bpy)_3]^{3+}$ or by Ce(IV), respectively, catalyzed by an all-inorganic molecular tetra-ruthenium polyoxometalate complex, $[\{Ru_4O_4(OH)_2(H_2O)_4\}(\gamma\text{-}SiW_{10}O_{36})_2]^{10-}$ (**1**). In our subsequent publication,[3] we demonstrated that **1** catalyzes water oxidation in a homogeneous visible-light-driven fashion using a sacrificial electron acceptor. In this reaction, the $[Ru(bpy)_3]^{3+}$ is generated using $[Ru(bpy)_3]^{2+}$ ($\gamma_{max} = 454$ nm) as a photosensitizer, and the persulfate ion, $[S_2O_8]^{2-}$, as the sacrificial electron acceptor (eq 1). Photoinduced oxidation of $[Ru(bpy)_3]^{2+}$ to $[Ru(bpy)_3]^{3+}$ by the persulfate ion has been well-studied in the literature[4] and is believed to proceed via a quenching of the visible-light-accessible metal-to-ligand charge transfer (MLCT) excited state. The products, $[Ru(bpy)_3]^{3+}$ and $SO_4^{-\bullet}$ (E_o, $SO_4^{-\bullet}/SO_4^{2-}$, ~2.4 V), are both strong oxidants, and the latter one may quickly oxidize another $[Ru(bpy)_3]^{2+}$ to a second $[Ru(bpy)_3]^{3+}$ (eq 2). The absorption of two photons and the consumption of 2 equiv of $[S_2O_8]^{2-}$ generates four $[Ru(bpy)_3]^{3+}$ that sequentially oxidize **1** by four electrons, which in its turn oxidizes two molecules of H_2O to O_2, thus regenerating $[Ru(bpy)_3]^{2+}$ (eq 3).

$$[Ru(bpy)_3]^{2+} + h\nu + [S_2O_8]^{2-} \rightarrow [Ru(bpy)_3]^{3+} + SO_4^{2-} + SO_4^{-\bullet} \quad (1)$$

$$[Ru(bpy)_3]^{2+} + SO_4^{-\bullet} \rightarrow [Ru(bpy)_3]^{3+} + SO_4^{2-} \quad (2)$$

$$4[Ru(bpy)_3]^{3+} + 2H_2O + \mathbf{1} \rightarrow 4[Ru(bpy)_3]^{2+} + O_2 + 4H^+ + \mathbf{1} \quad (3)$$

The goal of the present paper is two-fold. First, we study the electron transfer mechanism of reaction 1; namely, the absorption of a photon and transfer of one electron from an MLCT excited state of $[Ru(bpy)_3]^{2+}*$ to $[S_2O_8]^{2-}$ to yield $[Ru(bpy)_3]^{3+}$, $SO_4^{-\bullet}$, and SO_4^{2-}. In the literature, this process has been studied extensively using various experimental techniques.[4−19] On the basis of these thorough studies, two distinct mechanisms, called "unimolecular (or static quenching)" and "bimolecular (dynamic quenching)", have been proposed. The "unimolecular" mechanism results from the ground-state association of $[Ru(bpy)_3]^{2+}$ with $[S_2O_8]^{2-}$ to yield the $[Ru(bpy)_3]^{2+}\cdots[S_2O_8]^{2-}$ complex, although in the "bimolecular" mechanism, the initial photoin-

* Corresponding authors. E-mails: (A.L.K.) akaledi@emory.edu, (D.G.M.) dmusaev@emory.edu.

10.1021/jp908409n CCC: $40.75

duced electron transfer occurs in a collision between the excited $[Ru(bpy)_3]^{2+*}$ and $[S_2O_8]^{2-}$. An unusually strong dependence of bimolecular and unimolecular quenching rates on the solvent employed was reported.[4] This suggests that both quenching reactions occur by electron transfer and that the rate-limiting step in both mechanisms involves solvent reorganization of one or both reactants. In addition, it was shown that the optically bright excited **S1** state of $[Ru(bpy)_3]^{2+*}$ is extremely short-lived, with a lifetime of ~40 fs.[14] It is thought to undergo an efficient intersystem crossing via strong spin−orbit interaction to one of the lower-energy triplets.[10,12,14] These triplet states are believed to transfer the electron to persulfate. Below, we attempt to address these ideas.

In a noteworthy, very recent study, Youngblood et al.[20] reported electron transfer rates between a functionalized $[Ru(bpy)_3]^{2+}$ and IrO_2 nanoparticles. From their data, it can be inferred that in the complex of $[Ru(bpy)_3]^{2+*}$ with $[S_2O_8]^{2-}$, the electron transfer proceeds faster than ~30 ns.

The other goal of this paper is to find the optimal computational approach to study electron transfer in large, inorganic and organometallic systems. For this purpose, we validate the transition charge density model approach (vide infra).[21,22]

2. Computational and Experimental Methods

2.1. Computational Methods. Electronic structure and geometry optimizations of the ground singlet and the first triplet states of the $[Ru(bpy)_3]^{2+}\cdots[S_2O_8]^{2-}$complex as well as fragments $[Ru(bpy)_3]^{2+}$ and $[S_2O_8]^{2-}$ were performed at the B3LYP[23] level of theory in conjunction with the 6-31G(d) basis set augmented with diffuse s/p functions on the O and S atoms. For Ru, the Lanl2dz basis set and the corresponding ECP were used.[24] Excitation energies and excited state population analyses were performed using time-dependent DFT (TD-DFT) with the same functional (B3LYP) and basis sets. Note that the TD-DFT calculations of $[Ru(dcbpy)_2(NCS)_2]^{4-}$ yielded excited state energies and oscillator strengths in very good agreement with the available experimental data.[15] To include the solvation effects in water at 300 K and 1 atm, we performed single-point energy calculations (at the gas-phase optimized geometries) as well as partial geometry optimizations (for the selected systems; see below) with the polarizable continuum model (PCM)[25] using UFF atomic radii for all atoms. Most of the calculations were carried out with Gaussian-03;[26] spin−orbit coupling calculations[27] were performed using the Molpro-2008[28] program.

A Brief Description of the Transition Charge Density Model (TCDM). The *energy transfer probability*, per unit time, between the interacting ψ_m and ψ_n excited states (whose energies are in resonance) of $[Ru(bpy)_3]^{2+}$ and $[S_2O_8]^{2-}$, respectively, were assessed using Fermi's Golden Rule,

$$P_{mn} = (4\pi^2/h)|\langle\psi_m|V'|\psi_n\rangle|^2\,\delta(E_m - E_n) \qquad (4)$$

The matrix elements over the interaction potential V' are estimated on the basis of the transition charge density model.[21,22] This model assumes the interaction between the fragments is noncovalent and weak and utilizes a perturbation theory treatment. In this case, the interaction energy is given as a two-center Coulomb integral over the transition charge densities of the excited state m of fragment 1 and excited state n of fragment 2,

$$\langle\psi_m|V'|\psi_n\rangle \geq \int dr_1\, dr_2\, \frac{\rho_m(\mathbf{r}_1)\,\rho_n(\mathbf{r}_2)}{|\mathbf{r}_1 - \mathbf{r}_2|} \qquad (5)$$

where $\mathbf{r}_1$ and $\mathbf{r}_2$ are position vectors for the corresponding fragments. To simplify the calculation, the transition density can be discretized over atomic sites as $\rho_m(\mathbf{r}_1)\, d\mathbf{r}_1 \approx q_m(\mathbf{r}_1, i)$, where q_m is the transition charge of atom i for excited state m in fragment 1. Then the integral in eq 5 becomes a summation,

$$\langle\psi_m|V'|\psi_n\rangle \geq \sum_{i,j} \frac{q_m(\mathbf{r}_{1,i})\, q_n(\mathbf{r}_{2j})}{|\mathbf{r}_{1,i} - \mathbf{r}_{2,j}|} \qquad (6)$$

with i and j running over the atoms of the respective fragments. It was shown recently[22] that q_m is well-approximated by point charges obtained from a Mulliken population analysis.[29] In this work, we use a similar scheme to evaluate excited state interactions. We define $q_m(\mathbf{r}_1, i)$ for atom i of fragment 1 as the difference between the Mulliken charges of the excited state m and the ground state.

2.2. Experimental Methods. ***Materials.*** Tris(2,2′-bipyridyl)-dichlororuthenium(II) hexahydrate, henceforth $[Ru(bpy)_3]^{2+}$ and sodium persulfate (98+%) were purchased from Aldrich.

Steady-State Luminescence Quenching. Solutions of $[Ru(bpy)_3]^{2+}$, $[S_2O_8]^{2-}$, and their mixtures were prepared and stored in the dark to avoid photoreactions. All solutions were degassed with Ar before measurements. A 10 × 1 mm dual path-length quartz cuvette and 1.8-nm excitation and emission slits were used. Samples were excited at 450 nm, and emission intensity data were collected at 617−620 nm at 20 °C. The integration time was set at 0.05 s. To reduce photoinduced reactions during measurements, the light-exposure duration was minimized by decreasing the total acquisition time to less than 1 s. Repetitive spectral measurements showed that the emission intensity decreased by less than 2% during this acquisition time.

3. Results and Discussion

3.1. Geometry and Electronic States of the Reactants. The electronic properties of $[Ru(bpy)_3]^{2+}$ have been thoroughly studied.[4−19] $[Ru(bpy)_3]^{2+}$ absorbs UV light in the 420−520 nm (2.5−3 eV) wavelength range with a broad line shape, possibly having several bright states in the region; its three lowest singlet states are characterized as MLCT states involving one electron excitation from the Ru center to one of the three bpy ligands.[10−12,15] As seen in Table 1, our TD-DFT/PCM calculations of $[Ru(bpy)_3]^{2+}$ (fragment A) place its first six triplet states in the 2.56−2.88 eV range, and the singlet states slightly higher, at 2.74−2.95 eV. All these states are MLCT in character involving a d-orbital of Ru and π^*-orbital of one of the bpy ligands. For simplicity, we label these states of fragment A as **SAn**, and **TAn**, where **S** and **T** stand for singlet and triplet, respectively, and n = 1, 2, ..., 6.

TABLE 1: Excitation Energies of the Lower-Lying Singlet and Triplet States (in eV) of the Separated Reactants $[Ru(bpy)_3]^{2+}$ and $[S_2O_8]^{2-}$ (referred as A and B, respectively) Calculated at the TD-DFT/PCM and TD-DFT (in parentheses) Levels of Theory

	A: $[Ru(bpy)_3]^{2+}$		B: $[S_2O_8]^{2-}$	
n	**SAn**	**TAn**	**SBn**	**TBn**
1	2.7375 (2.7206)	2.5589 (2.5680)	5.1942 (4.7361)	4.1160 (3.6625)
2	2.7390 (2.8012)	2.5654 (2.6313)	5.7974 (5.3695)	5.3904 (5.2363)
3	2.7503 (2.8320)	2.6099 (2.6413)	5.8077 (5.3714)	5.6693 (5.2381)
4	2.9214 (2.8672)	2.8153 (2.7448)	6.2532 (5.5606)	5.6789 (5.3115)
5	2.9500 (2.9027)	2.8311 (2.7897)	6.5582 (5.7317)	6.1080 (5.4205)
6	2.9521 (2.9720)	2.8793 (2.8388)	6.6323 (5.7383)	6.2630 (5.6454)

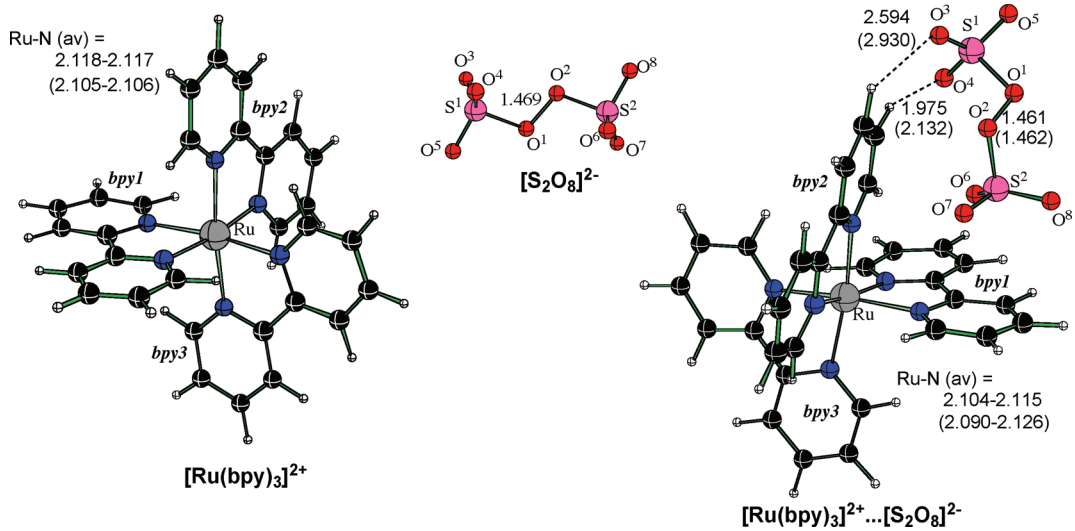

Figure 1. The calculated structures (for the ground singlet states) and important geometry parameters (in Å) of $[Ru(bpy)_3]^{2+}$, $[S_2O_8]^{2-}$, and $[Ru(bpy)_3]^{2+}\cdots[S_2O_8]^{2-}$. Numbers given in parentheses are for triplet electronic states.

The nature of the **SA0**−**TA1** transition is consistent with the optimized geometries of $[Ru(bpy)_3]^{2+}$ at these states. As seen in Figure 1, this transition (as well as the expected **SA0**−**SA1**, **SA0**−**SA2**, **SA0**−**SA3**, **SA0**−**TA2**, and **SA0**−**TA3** transitions) does not change the geometry of the system significantly. For example, upon **SA0**−**TA1** transition, the calculated average Ru−N bond distances change only slightly, from 2.118−2.117 Å to 2.090−2.126 Å. These conclusions are consistent with results of Chergui and co-workers[17] based on femtosecond laser/X-ray coupled spectroscopy studies.

The excited states of $[S_2O_8]^{2-}$ (called as fragment B; similarly, we label electronic states of fragment B as **SBn**, and **TBn**) are less studied. Using sophisticated computational methods, McKee reported[30] that the vertical ionization potential of $[S_2O_8]^{2-}$ is 1.56 eV in the gas phase. Its first excited state is expected to be repulsive, since the excitation takes place to the antibonding π^*-orbital of the bridging peroxo (O−O) bond, which results in dissociation of $[S_2O_8]^{2-}$ into two $SO_4^{-\bullet}$ radicals. Our TD-DFT/PCM calculations of $[S_2O_8]^{2-}$ performed at the geometry of its **SB0** state show that its first excited state is a triplet state (**TB1**) at 4.12 eV. Then follows a singlet state (**SB1**) at 5.19 eV and another triplet (**TB2**) state at 5.39 eV (see Table 1 for the calculated six lowest singlet and triplet states of $[S_2O_8]^{2-}$, fragment B).

As seen in Table 1, excited states of fragments $[Ru(bpy)_3]^{2+}$ and $[S_2O_8]^{2-}$ are far off resonance at their respective B3LYP/PCM optimized [for the **SA0** and **TA1**] equilibrium geometries. Electron transfer between the $[Ru(bpy)_3]^{2+}$ and $[S_2O_8]^{2-}$, on the other hand, is expected to occur at geometries where the two fragments share similar excitation energies. As we show below (see Section 3.3), elongation of the O−O peroxo bond of $[S_2O_8]^{2-}$ lowers the persulfate excitation energy and brings it closer to that of $[Ru(bpy)_3]^{2+}$.

3.2. The Low-Lying Excited States of the $[Ru(bpy)_3]^{2+}\cdots[S_2O_8]^{2-}$ Complex. In this section, we describe the low-lying electronic states of the $[Ru(bpy)_3]^{2+}\cdots[S_2O_8]^{2-}$complex. These states, most likely, will be involved in $O_3SO-OSO_3$ photoinduced O−O bond cleavage dynamics. The geometry of its ground singlet state, **S0**, and the first triplet excite state, **T1**, are shown in Figure 1. As seen from this Figure, the geometries of the $[Ru(bpy)_3]^{2+}$ and $[S_2O_8]^{2-}$ fragments in the complex $[Ru(bpy)_3]^{2+}\cdots[S_2O_8]^{2-}$ and in their free (i.e. noninteracting) states, respectively, are very similar. This indicates that the nature of the interaction between these fragments is noncovalent in character, even though the calculated $[Ru(bpy)_3]^{2+}\cdots[S_2O_8]^{2-}$ complexation energy is −211 kcal/mol in the gas phase. Indeed, as seen from Figure 1, the closest H-bonding distance between these fragments is 1.975 (2.132) Å. Furthermore, most of this energy can be recovered by the simple Coulomb formula, $q1 \times q2/R = -204$ kcal/mol, where $q1 = +2$, $q2 = -2$, and $R =$ 6.5 Å (the distance between the Ru and the center of the O−O peroxo bond). Placing the system in an aqueous medium is expected to destabilize the interaction because of dielectric shielding. In fact, a DFT/PCM optimization starting from the gas phase structure reduces complexation energy to only −2.1 kcal/mol. This result shows the importance of solvent effect in defining $[Ru(bpy)_3]^{2+}-[S_2O_8]^{2-}$ bonding energy. Since the nature of this bond is electrostatic, one would expect a strong solvent dependence.

TABLE 2: Vertical Excitation Energies (relative to S0, in eV) of the $[Ru(bpy)_3]^{2+}\cdots[S_2O_8]^{2-}$ Complex Calculated at the TD-DFT Level of Theory in the Gas Phase (GP) and in Aqueous Solution (PCM), As Well As at the Transition Charge Density Model (TCDM) Level[a]

state	ΔE(GP)	ΔE(PCM)	ΔE(TCDM/PCM)	DTM
T1/T1′	0.5082	2.5474[c]	2.5172	0.0
T2/T2′	0.7563	2.6024	2.5497	0.0
S1/S1′	0.5083	2.6354	2.6645	0.228
S2/S2′	0.7564	2.6845	2.7123	0.254

[a] Dipole transition moments (DTM, in Debye) for these states of $[Ru(bpy)_3]^{2+}\cdots[S_2O_8]^{2-}$ complex are calculated at the TD-DFT level. [b] We label the approximate excited states of $[Ru(bpy)_3]^{2+}\cdots[S_2O_8]^{2-}$ calculated at the TCDM level with a "prime"; i. e., **S1′**, **T1′**, etc., which correlates with the TD-DFT-calculated **S1**, **T1**, etc. states, respectively. [c] B3LYP calculated adiabatic excitation energy of **T1** is 2.50 eV.

As seen in Table 2, the hydration of $[Ru(bpy)_3]^{2+}\cdots[S_2O_8]^{2-}$ greatly affects the calculated vertical excitation energies. For example, the **S0**−**S1** and **S0**−**S2** energy splittings in $[Ru(bpy)_3]^{2+}\cdots[S_2O_8]^{2-}$ increase by approximately 2 eV (from 0.5083 and 0.7564 eV to 2.6354 and 2.6845 eV, respectively) upon going from the gas phase to aqueous solution. A similar trend is observed for the calculated energy difference between the **S0** and triplet **T1** and **T2** states of $[Ru(bpy)_3]^{2+}\cdots[S_2O_8]^{2-}$. The PCM-calculated energy gap between the ground singlet and lower-lying excited singlet and triplet states of $[Ru(bpy)_3]^{2+}$ (see

Table 1) and $[Ru(bpy)_3]^{2+}\cdots[S_2O_8]^{2-}$ are consistent with UV experiments,[5] which use photon wavelengths in the range of 420−520 nm (2.9−2.4 eV) to create the excited state of $[Ru(bpy)_3]^{2+}$.

The two likely candidates for the initial photon absorption in $[Ru(bpy)_3]^{2+}\cdots[S_2O_8]^{2-}$ (as in free $[Ru(bpy)_3]^{2+}$) are **S1** and **S2** states, both of which have sizable dipole transition moments, 0.228 and 0.254 D, respectively. The main electronic nature of the **S0** → **S1** and **S0** → **S2** excitations is MLCT, during which a single electron from the Ru d-orbitals is promoted to the antibonding π^*-orbital one of the bpy ligands. In the case of **S1**, the electron transfer takes place to the bpy1 ligand nonadjacent to persulfate, with a minor mixing of excitation to an adjacent bpy2. The **S2** state shows a similar characteristic, but with a stronger involvement of the adjacent bpy2 ligand.

The first triplet **T1** state of $[Ru(bpy)_3]^{2+}\cdots[S_2O_8]^{2-}$ (like in $[Ru(bpy)_3]^{2+}$) shares a very similar excitation character with the **S1** state. This is true because **S1/T1** pairs in the Franck−Condon region typically arise from the same spatial configuration but differ by direction of spin. The vertical **S0** → **T1** excitation energy for $[Ru(bpy)_3]^{2+}\cdots[S_2O_8]^{2-}$, 2.55 eV, is slightly lower than that of **S0** → **S1**, as expected. The second triplet **T2** state of $[Ru(bpy)_3]^{2+}\cdots[S_2O_8]^{2-}$ has a much more delocalized excitation vector than the **T1** state, involving at least eight components of comparable magnitude. It mimics the **S2** state, where the electron is promoted predominantly from the Ru-center to bpy2 ligand. Energetically, the **T2** state is lower than the **S1** and **S2** states, which favors its involvement in dissociation dynamics.

As a means of calibrating the accuracy of TD-DFT/PCM for the excited states, we performed a single-point energy calculation of the **T1** state using the regular B3LYP/PCM approach, which yielded an 2.5 eV **S0** → **T1** excitation energy for $[Ru(bpy)_3]^{2+}\cdots[S_2O_8]^{2-}$ complex. The error is relatively small, and we can assume that TD-DFT will not overestimate other excitation energies by more than 0.05 eV.

3.3. $[Ru(bpy)_3]^{2+}$ and $[S_2O_8]^{2-}$ Interaction Model in the Franck−Condon Region. None of the above-described low-lying excited states of $[Ru(bpy)_3]^{2+}\cdots[S_2O_8]^{2-}$show an appreciable component of electron transfer from $[Ru(bpy)_3]^{2+}$ to the persulfate because they are dominated by Ru → ligand (bpy) transitions. At this point, it may be insightful to analyze the character of these excited states using the transition charge density model (TCDM) outlined in the Introduction and Computational Methods parts. We note that the first excitation energy, **S0** → **S1**, is calculated to be 2.55 eV, which is much greater than the $[Ru(bpy)_3]^{2+}\cdots[S_2O_8]^{2-}$ → $[Ru(bpy)_3]^{2+}$ + $[S_2O_8]^{2-}$ dissociation energy of 2.1 kcal/mol. This allows us to use perturbation theory for exciton interaction between $[Ru(bpy)_3]^{2+}$ and $[S_2O_8]^{2-}$, as described in eqs 4−6.

To this end, to estimate the exciton interaction between $[Ru(bpy)_3]^{2+}$ and $[S_2O_8]2-$ (i.e., fragments A and B) we construct a small interaction Hamiltonian consisting of 6 excited singlet and 6 excited triplet states of each fragment, a 12 × 12 matrix for each spin symmetry. The diagonal elements of this matrix are the excitation energies of the individual fragments (zero-order energies) calculated at the geometry of the complex $[Ru(bpy)_3]^{2+}\cdots[S_2O_8]^{2-}$ using the TD-DFT/PCM method. The off-diagonal elements are computed using eq 5. To clarify this protocol, we show as an example a 4 × 4 matrix for singlet states of fragments A and B in Figure 2.

The first on-diagonal block of this matrix consists of the zero-order states of fragment A; the second on-diagonal block consists of zero-order states of fragment B. The states within a block

	SA1	SA2	SB1	SB2
SA1	$E_1(A)$	0	$V'_{11}(AB)$	$V'_{12}(AB)$
SA2	0	$E_2(A)$	$V'_{21}(AB)$	$V'_{22}(AB)$
SB1	$V'_{11}(BA)$	$V'_{12}(BA)$	$E_1(B)$	0
SB2	$V'_{21}(BA)$	$V'_{22}(BA)$	0	$E_2(B)$

Figure 2. A 4 × 4 interaction matrix for singlet states (given as an example) of fragments A ($[Ru(bpy)_3]^{2+}$) and B ($[S_2O_8]^{2-}$). For triplet states, an independent interaction Hamiltonian is set up in similar fashion using **TA1**, **TA2**, **TB1**, and **TB2** as basis.

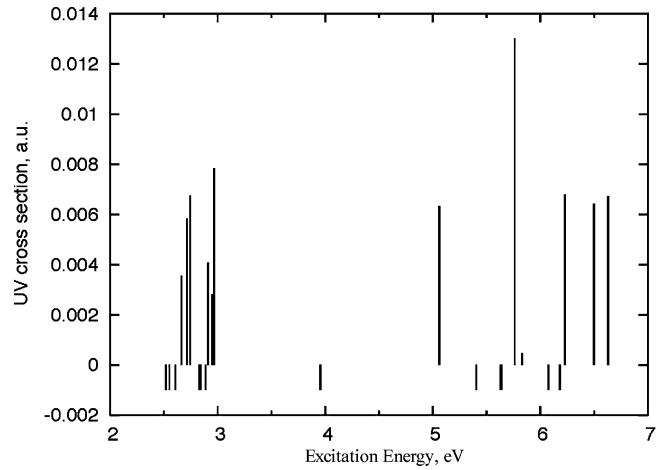

Figure 3. The UV absorption cross section in (e•Bohr)^2 for the singlet states of $[Ru(bpy)_3]^{2+}\cdots[S_2O_8]^{2-}$ in the Franck−Condon region, calculated at the TD-DFT and transition charge model levels. The triplet positions are marked with uniform arbitrary negative absorption values. The $[Ru(bpy)_3]^{2+}$ MLCT states are localized in the 2.5−3 eV regime.

cannot interact with each other directly, but can interact only through the elements of the off-diagonal block V′. The eigenvalues of this matrix are approximate excitation energies of the complex, whereas its eigenvectors show the order of mixing of the states of fragments A and B and reveal the nature of the interactions. Note that below, we label the approximate excited states of $[Ru(bpy)_3]^{2+}\cdots[S_2O_8]^{2-}$ calculated at the TCDM level with a "prime", i. e., **S1′** correlates with **S1**, **T1′** correlates with **T1**, etc. As seen in Table 2, the TCDM/PCM approach provides the excitation energies that are very close to that calculated at the TD-DFT/PCM level: the difference between the TCDM/PCM and TD-DFT/PCM calculated values of the excitation energies of $[Ru(bpy)_3]^{2+}\cdots[S_2O_8]^{2-}$ is within 0.03−0.05 eV.

Using the results of TCDM calculations, we can recover the approximate UV spectrum of the complex, shown here in Figure 3.

The positions of the "sticks" are the TCDM excitation energies, and the heights (cross sections) are calculated as an average over eigenvector components of individual fragments. We note that since only six states of each fragment were included in the calculation, some bright states could be missing between 3 and 5 eV.

Mulliken transition charges (calculated as a difference of Mulliken charges of a given electronic state and **S0**), which were used to calculate the components of the interaction matrix, are presented in Table 3.

TABLE 3: The Calculated Mulliken Transition Charges (in e) of Atoms or Ligands (Summed over Atoms) in $[Ru(bpy)_3]^{2+}$ and $[S_2O_8]^{2-}$

(a) For Fragment A: $[Ru(bpy)_3]^{2+}$

atoms/ligands	SA1	SA2	SA3	TA1	TA2	TA3
Ru	0.769	0.783	0.816	0.665	0.676	0.680
bpy1	−0.053	−0.745	0.007	−0.121	−0.384	−0.176
bpy2	−0.190	−0.050	−0.554	−0.042	−0.313	−0.322
bpy3	−0.521	0.011	−0.267	−0.502	0.021	−0.184

(b) For Fragment B: $[S_2O_8]^{2-}$

	SB1	SB2	SB3	TB1	TB2	TB3
O^5	0.027	0.012	0.377	0.009	0.009	0.239
S^1	−0.095	−0.129	−0.279	−0.058	−0.058	−0.258
O^3	0.029	−0.001	0.320	0.012	0.012	0.177
O^4	0.036	−0.002	0.315	0.021	0.021	0.161
O^1	0.001	−0.354	−0.287	0.018	0.018	−0.289
O^2	0.000	−0.289	−0.350	0.011	0.011	−0.296
S^2	−0.092	−0.266	−0.123	−0.056	−0.056	−0.226
O^8	0.024	0.373	0.019	0.008	0.008	0.200
O^6	0.040	0.321	0.004	0.023	0.023	0.139
O^7	0.030	0.335	0.005	0.012	0.012	0.153

Diagonalization of the interaction matrix and analysis of its eigenvectors reveal that the **S1′** state (i.e., the **S1** state) of $[Ru(bpy)_3]^{2+}\cdots[S_2O_8]^{2-}$ is composed primarily of **SA1** (76%) and **SA2** (14%), whereas the **S2′** state is dominated by **SA2**, with an 83% contribution and involving 21% of **SA1**; the **S3′** state is mainly **SA3** with an 85% weight of fragment A (e.g., $[Ru(bpy)_3]^{2+}$). The corresponding triplets are almost unmixed at the equilibrium geometry and represent the first three triplet states of $[Ru(bpy)_3]^{2+}$. Thus, all six lower-lying electronic states (**S1′/S1**, **S2′/S2**, **S3′/S3**, **T1′/T1**, **T2′/T2**, and **T3′/T3**, states) of $[Ru(bpy)_3]^{2+}\cdots[S_2O_8]^{2-}$ originate mainly from the $[Ru(bpy)_3]^{2+}$ (fragment A) with no mixture from the persulfate (fragment B). All excited states of the latter lie much higher in energy at the equilibrium geometry of the complex.

3.4. Mechanism of Exciton Transfer from $[Ru(bpy)_3]^{2+}$* to $[S_2O_8]^{2-}$ and Homolytic O−O Bond Cleavage. The computational data presented above fully support and provide insights into the two distinct mechanisms, called "unimolecular" and "bimolecular", previously predicted for electron transfer from $[Ru(bpy)_3]^{2+}$* to $[S_2O_8]^{2-}$ resulting in $[Ru(bpy)_3]^{3+} + SO_4^{2-} + SO_4^{-}$. Energies (and other details) of these mechanisms are given in Figure 4.

As seen in Figure 4, the "unimolecular" mechanism starts with a formation of the $[Ru(bpy)_3]^{2+}\cdots[S_2O_8]^{2-}$ complex in its ground **S0** state, followed by the photoexcitation of the system. Since the initial photon absorption by the complex promotes it to the optically bright **S1** state, there has to be a nonradiative transition from **S1** to **T1** to observe the charge transfer products. The spin-forbidden transition can be facilitated by spin−orbit coupling, which is expected to be strong due to the presence of a heavy element. From our analysis presented above, the **S1**, **S2**, **T1**, and **T2** excited states of $\{[Ru(bpy)_3]^{2+}\cdots[S_2O_8]^{2-}\}$* in the Franck−Condon region are characterized as pure $[Ru(bpy)_3]^{2+}$* states. It is well-known from experiments that the bright singlet **SA1** state of $[Ru(bpy)_3]^{2+}$* is extremely short-lived, with a lifetime of ∼40 fs.[14] This implies that the **SA1** state of $[Ru(bpy)_3]^{2+}$* decays in the early stages of the dynamics before the system has had the time to leave the Franck−Condon region. This phenomenon is expected to be very similar for the $[Ru(bpy)_3]^{2+}\cdots[S_2O_8]^{2-}$ complex and $[Ru(bpy)_3]^{2+}$ because of a relatively weak interaction between the $[Ru(bpy)_3]^{2+}$ and $[S_2O_8]^{2-}$ fragments. Therefore, to gain insight into the **S1/T1** transition in the excited complex $\{[Ru(bpy)_3]^{2+}\cdots[S_2O_8]^{2-}\}$*, we estimate the spin−orbit coupling in $[Ru(bpy)_3]^{2+}$*, which is computationally less demanding. For this purpose, we calculated a few key matrix elements over the L•S operator using an MC-SCF wave function and an all-electron minimal basis set. (One should note that the limited computational approach used here will, most likely, underestimate the calculated spin−orbit coupling. However, the ratios of these matrix elements are expected to be qualitatively correct; hence, we are confident in reporting on the relative transition probability between the **S1/T1** and **S1/T2** channels.) An active space of four electrons in four orbitals was used for a 2-singlet/2-triplet state averaged calculation. Table 4 shows the four groups of interactions: **S1/T1**, **S1/T2**, **S0/T1**, and **S0/T2**.

TABLE 4: Complex Matrix Elements (in cm^{-1}) of the L•S Spin-Orbit Operator for $[Ru(bpy)_3]^{2+}$ in the Franck-Condon Region, Calculated at the MC-SCF Level of Theory[a]

	|TA1, 1+>	|TA1, 0>	|TA1, 1−>	|TA2, 1+>	|TA2, 0>	|TA2, 1−>
<**SA1**, 0|	−0.3	−1.4*i*	5.2*i*	30.4	−57.3*i*	−26.6*i*
<**SA0**, 0|	−242.8	559.1*i*	269.8*i*	−4.0	−205.2*i*	437.4*i*

[a] The M_s quantum numbers are shown after the comma for each spin state.

As expected, **S0** is coupled to the triplet states much more strongly than is the **S1** state. This is due to the fact that **SA0**'s spatial configuration is very different from those of the triplet

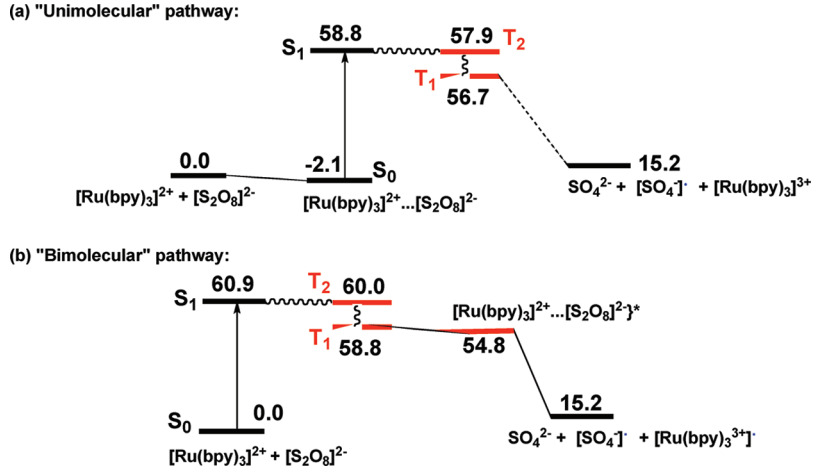

Figure 4. The two proposed mechanisms of photoinduced electron transfer between $[Ru(bpy)_3]^{2+}$ and $[S_2O_8]^{2-}$. The relative energies are in kcal/mol.

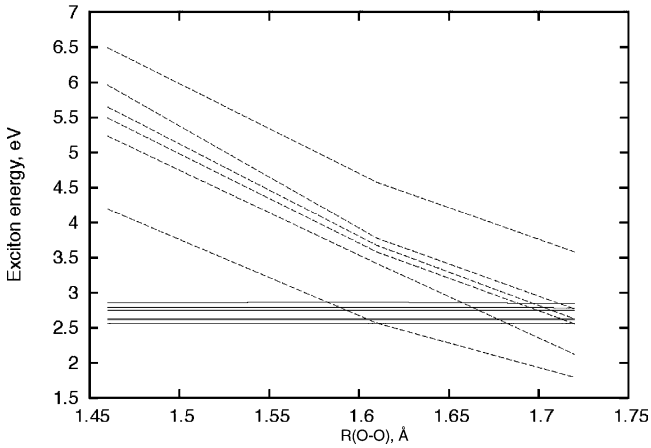

Figure 5. Dependence of exciton energies on the persulfate O−O stretch: the solid lines are for $[Ru(bpy)_3]^{2+}$, and the dashed lines for are $[S_2O_8]^{2-}$. Only the triplet states are shown.

states, which, like **S1**, are MLCT states. We note, however, that the **S0** state is unlikely to be involved in the dynamics, given the large energy gap with the excited states. Of the other two pairs of interest, **S1/T2** appears to have a much more efficient intersystem crossing; the rms magnitude of the matrix element is 70.1 cm^{-1}, as compared with only 5.4 cm^{-1} for **S1/T1**. (We have defined rms as the square root of the sum of the squares of the three magnetic components of a triplet; cf. Table 4.) Because probabilities are proportional to squares of the matrix elements, the **S1/T2** channel appears almost 200 times more efficient than **S1/T1**. This result indicates that **T2** is most likely involved in photodissociation of the O−O peroxo bond at the early stages serving as an intermediate in the **S1** → **T2** → **T1** chain, where the second step is the highly efficient (spin-allowed) internal conversion. Once the system has converted to **T1**, it can evolve toward dissociation. Although the spin−orbit calculations for the singlet/triplet state pairs were performed away from their seams of crossing, the main conclusion drawn here should not change, since spin−orbit coupling is usually not very sensitive to geometrical variations.

However, as we have shown above, the lower-lying **S1**, **T1**, and **T2** electronic states of the excited $\{[Ru(bpy)_3]^{2+}\cdots[S_2O_8]^{2-}\}^*$ originate mainly from the $[Ru(bpy)_3]^{2+*}$ (fragment A): no mixture from the persulfate (fragment B), all excited states of which lie much higher in energy at the equilibrium geometry of the complex. For the $[Ru(bpy)_3]^{2+*} \rightarrow [S_2O_8]^{2-}$ charge transfer take place in $\{[Ru(bpy)_3]^{2+}\cdots[S_2O_8]^{2-}\}^*$, it is necessary to bring the zero order states of the $[Ru(bpy)_3]^{2+*}$ and $[S_2O_8]^{2-}$ fragments into (near) resonance. Our numerous exploratory TD-DFT/PCM calculations of $[Ru(bpy)_3]^{2+}\cdots[S_2O_8]^{2-}$ at different O−O peroxo bond distances reveal that the excited states of the persulfate will be lowered when the O−O peroxo bond is elongated. The performed relaxed scan of the O−O bond in the gas phase followed by single-point TD-DFT/PCM calculations at the resulted geometries show that the R(O−O) = 1.72 Å is one of the more optimal geometries for resonant transitions between the few lowest singlet states on each fragment. Similarly, we located R(O−O) = 1.61 Å as the most optimal value for the triplet states. Results for the triplet states are detailed in Figure 5.

It has been mentioned above that **S1** of $[Ru(bpy)_3]^{2+*}$ is short-lived; thus, it is doubtful that any significant population of it will remain while the vibrational wavepacket of $[S_2O_8]^{2-}$ samples the elongated O−O bond. The **T1** state of $\{[Ru(bpy)_3]^{2+}\cdots[S_2O_8]^{2-}\}^*$, on the other hand, is long-lived and can traverse ~0.15 Å along O−O to reach "transition" point. Here, we concentrate only on those triplet pairs whose energy difference at R(O−O) = 1.61 Å is $E_m - E_n \approx 0.1$ eV, so as to approximately satisfy the resonance condition of eq 3. The only pair which satisfies this condition at the transition geometry is **TA1−TB1**; its interaction matrix element is 0.023 eV. Recall that **TA1** is an excitation from Ru to bpy1, and TB1 is a nonpolar excitation in the distended $SO_4^- - SO_4^-$ molecule.

TABLE 5: The Triplet State Energies (in eV) of the $\{[Ru(bpy)_3]^{2+}\cdots[S_2O_8]^{2-}\}^*$ Complex at the Charge "Transition" Point (where R(O−O) = 1.6159 Å)[a]

state	configuration	ΔE (TD-DFT)[c]	ΔE (TCDM)[c]	$P_{AB}^{T1'}$	lifetime
T1/T1′	0.447 TA1 −0.892 TB1	1.9391	1.9774	0.835	47
T2/T2′	0.891 TA1 +0.447 TB1	1.9986	2.0354	0.832	47

[a] The calculated transition probabilities (in eV/ps) and lifetime (in ns) of the electron transfer between the fragments A ($[Ru(bpy)_3]^{2+}$) and B ($[S_2O_8]^{2-}$) are also given. [b] The average density of exit states is 3 eV^{-1}, as seen in Figure 5. [c] These values include solvent (water) effects at the PCM level.

It is useful to introduce the *cumulative* probability of electron transfer between fragments A and B. We define this quantity as follows, for eigenstate **T1/T1′**:

$$P_{AB}^{T1'} = (4\pi^2/h)\sum_{mn}(c_n^{B*}\, c_m^{A})^2 |\langle TB_n|V'|TA_m\rangle|^2\, \delta(E_m - E_n) \tag{7}$$

where c_n^B/c_m^A is the n-th/m-th component of eigenvector **c** overlapping with fragment B/A. The delta function ensures that only resonant pairs contribute. The leading factor inside the double sum is proportional to what we refer to as the *pair involvement coefficient*,

$$\alpha_{mn}^{T1'} = 4(c_n^{B*}\, c_m^{A})^2$$

which is simply the square of the density matrix off-diagonal elements $m \neq n$. (Recall that due to the normalization condition of

$$\sum_m |c_m^A|^2 + \sum_n |c_n^B|^2 = 1$$

the maximum value of $\alpha_{mn}^{T1'}$ is 1 (for example, when $c_m^A = c_n^B = 1/\sqrt{2}$), whereas for all other indices, k, $c_k^{A/B} = 0$). In other words, both c_m^A and c_n^B have to be large for the *pair involvement coefficient* to be sizable. The cumulative probability is rewritten in terms of pair involvement coefficients and the state-to-state probabilities (eq 4),

$$P_{AB}^{T1'} = (1/4)\sum_{mn}\alpha_{mn}^{T1'} P_{mn}^{AB} = (1/4)\mathrm{tr}[\alpha^{AB} P^{AB}] \tag{8}$$

The only nonzero cumulative transition probabilities were found for **T1** and **T2**, which are summarized in Table 5.

The higher triplet states appear noninvolved in energy transfer. This is explained by their nearly vanishing pair involvement coefficient for the only near-resonant pair at the "transition" geometry, **TA1−TB1**. To compare, $\alpha_{TA1-TB1}^{T1'} = 0.6359$ and $\alpha_{TA1-TB1}^{T2'} = 0.6345$, whereas $\alpha_{TA1-TB1}^{Tj'} = 0$, for $j = 3, 4, \ldots$.

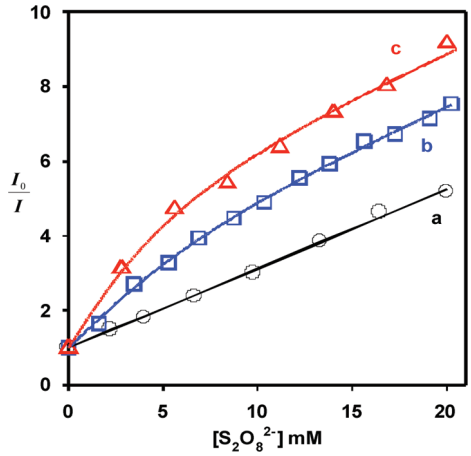

Figure 6. Stern−Volmer plot for solutions containing (a) 200 mM pH 7.2 phosphate buffer, (b) 20 mM pH 7.2 phosphate buffer, and (c) no buffer. All solutions contained 1 mM $[Ru(bpy)_3]^{2+}$ and were purged with Ar. Solid line drawn through curves b and c was calculated from eq 10 (see text).

We can now estimate the lifetime of the electron transfer process. Inspecting Figure 5, we notice that all six $[S_2O_8]^{2-}$ triplets fall within a 2 eV window throughout the O−O distance. This suggests the average density of states to be $\rho \approx 3$ eV^{-1}. Further, we assume that the O−O peroxo bond activation is mediated by the thermal energy of the solvent. Thus, the rate should be proportional to the usual Boltzmann factor, $\exp(-\Delta E/kT)$, where $\Delta E = 6.9$ kcal/mol is the change in ground state energy of $S_2O_8^{2-}$ (in water) at the "transition point" (O−O = 1.61 Å). Using the relationship "rate" ∝ "probability" × "density-of-states", we scale eq 3 by the density of states and the exponential factor evaluated at 300 K, invert the result, and obtain a lifetime of 47 ns for **T1** and a very similar number for **T2**. This value is comparable to the upper limit of 30 ns that can be inferred from experiment.[20]

The alternative mechanism, referred to as "bimolecular", does not assume formation of complex $[Ru(bpy)_3]^{2+}\cdots[S_2O_8]^{2-}$ in its **S0** state. Instead, the initial photon excites $[Ru(bpy)_3]^{2+}$ to **S1** (**SA1** in our nomenclature) which, in similar fashion to the "unimolecular" mechanism, decays to **T1** (**TA1**). The long-lived **T1** state of $[Ru(bpy)_3]^{2+*}$ interacts with $[S_2O_8]^{2-}$ via thermally induced collisions, and electron transfer takes place via the same pathway as was discussed above for the "unimolecular" mechanism. Under typical experimental conditions, both of these mechanisms are likely to compete with each other. This competition depends on concentrations, ionic strength (or buffer conditions), solvent composition (e.g., ratio of CH_3CN and H_2O), and other factors.

3.5. Quenching of $[Ru(bpy)_3]^{2+*}$ in Aqueous Solutions by $[S_2O_8]^{2-}$ Using the Steady-State Luminescence Techniques. To clarify the mechanism of reaction 1 under the experimental conditions reported in our previous paper,[3] we have studied quenching of $[Ru(bpy)_3]^{2+*}$ in aqueous solutions by $[S_2O_8]^{2-}$ using the steady-state luminescence techniques at three different buffer concentrations: (a) 0.2 M pH 7.2 sodium phosphate buffer, (b) 20 mM pH 7.2 sodium phosphate buffer, and (c) no buffer. Buffer b was used in our previous study of photodriven water oxidation reaction.[3] The Stern−Volmer (SV) plots, I_0/I vs $[S_2O_8]^{2-}$ (where I and I_0 and are the emission internsity of $[Ru(bpy)_3]^{2+*}$ in the presence and absence of the quencher, respectively), are shown in Figure 6. The SV plot for the solution containing high buffer concentration (buffer a) yields a linear line with a unity intercept. The SV plot

TABLE 6: Results of Kinetics Fitting of the $[Ru(bpy)_3]^{2+}\cdots[S_2O_8]^{2-}$]

buffer (mM)	τ' (ns)	$k_q(k_q')$ (M^{-1} s^{-1})	K_{eq} (M^{-1})	k_{ET} (s^{-1})	α
0	108	3.9×10^8	6.93×10^2	7.4×10^6	0.75
20	149	3.9×10^8	3.53×10^2	4.9×10^6	0.61
200	NA	3.9×10^8	0	NA	0

significantly deviates from linearity and curves downward in solutions with 0 and 20 mM buffer.

The SV plot for buffers a and c are similar to results previously reported by Bard and co-workers for the same emitter and quencher in a different electrolyte.[4] They showed that the SV plot can be well-described by a model that takes into account the formation of ground-state ion pairs between the emitter and the quencher. This model gives rise the following equation for emission quenching:[4]

$$\frac{I_0}{I} = \frac{(1 + K_{eq}[S_2O_8]^{2-})(1 + k_q\tau_0[S_2O_8]^{2-})}{1 + \frac{\tau'}{\tau_0}\frac{K_{eq}([S_2O_8]^{2-})(1 + k_q\tau_0[S_2O_8]^{2-})}{1 + k_q'\tau_0'[S_2O_8]^{2-}}} \quad (9)$$

where K_{eq} is the equilibrium constant of ion pair formation; τ_0 (τ') and k_q (k_q') are the unimolecular decay time and the bimolecular quenching constant of the excited emitter in free form (ion pair state), respectively. Under conditions of negligible ion-pair formation, $K_{eq}[S_2O_8]^{2-} \ll 1$, eq 9 is simplified to[4]

$$\frac{I_0}{I} = 1 + k_q\tau_0[S_2O_8]^{2-} \quad (10)$$

As shown in Figure 6, curve a can be well fit by eq 10, suggesting that under high buffer concentration, the equilibrium constant is negligible and most quenchers are not in the ion-pair state. The quenching proceeds through the bimolecular pathway. The slope of the linear fit gives the value of $k_q\tau_0$ of 212 M^{-1}. Using the reported $[Ru(bpy)_3]^{2+*}$ lifetime,[4] τ_0, of 0.55 ms, we obtain a k_q of 3.9×10^8 M^{-1} s^{-1}. Deviation from linearity of the SV plots at low (or no) buffer concentration (curve c and b) indicates the formation of a ground-state ion pair between $[Ru(bpy)_3]^{2+}$ and $[S_2O_8]^{2-}$. Assuming that k_q and k_q' are similar,[4] these SV plots can be fitted by eq 9, as shown in Figure 6. The results of the fitting are listed in Table 6.

The intrinsic radiative and nonradiative rate constants of $[Ru(bpy)_3]^{2+*}\cdots[S_2O_8]^{2-}$ should be similar to the $[Ru(bpy)_3]^{2+*}$ due to the weak (a few kilocalories per mole) electrostatic interaction between $[Ru(bpy)_3]^{2+}$ and $[S_2O_8]^{2-}$. Then, the photoinduced unimolecular ET rate (k_{ET}) in eq 11 can be estimated as

$$k_{ET} = \frac{1}{\tau'} - \frac{1}{\tau_0} \quad (11)$$

The estimated k_{ET} is $\sim 7.4 \times 10^6$ s^{-1} in solutions without buffer. This result is in qualitative agreement with the computed unimolecular ET rate. At the buffer concentration used in our photodriven water oxidation experiment (buffer b), the k_{ET} is $\sim 4.9 \times 10^6$ s^{-1}. At 5 mM $[S_2O_8]^{2-}$, the bimolecular ET rate $k_q[S_2O_8]^{2-}$ is $\sim 1.9 \times 10^6$ s^{-1}. Under these conditions, the unimolecular ET rate is 2.5 times faster than the bimolecular pathway, suggesting that formation of an ion pair facilitates generation of the oxidant $[Ru(bpy)_3]^{3+}$. Additionally, the result-

ing equilibrium constant, K_{eq}, from the fittings can be used to estimate the percentage of the emitters that forms the ion pair in the ground state (α). For example, at 5.0 mM $Na_2S_2O_8$, α is 0.61 in 20 mM sodium phosphate buffer solution and 0.75 in the absence of buffer. Thus, under the experimental conditions (in aqueous solution and at pH 7.2 and 20 mM sodium phosphate buffer) reported in our previous paper, 61% of $[Ru(bpy)_3]^{2+}$* quenching by $[S_2O_8]^{2-}$ occurs via a formation of an ion-pair complex $[Ru(bpy)_3]^{2+*}\cdots[S_2O_8]^{2-}$. As shown in Figure 6, the ratio of I_0/I increases with decreasing buffer concentration at constant $[S_2O_8]^{2-}$, suggesting that the phosphate buffer deactivates the quenching process by inhibiting formation of the ground-state ion pair.

4. Conclusions

Photoinduced (420−520 nm wavelength range) electron transfer between $[Ru(bpy)_3]^{2+}$ and $[S_2O_8]^{2-}$ resulting in the formation of $[Ru(bpy)_3]^{3+}$ and O−O bond cleavage is a complex process which includes both "unimolecular" and "bimolecular" pathways, in agreement with the previous experimental findings. This distinction arises due to a weak interaction between the two reactants. Analysis of excited electronic states and their spin−orbit mixing suggests that a photon excites an MLCT **SA1/S1** state of $[Ru(bpy)_3]^{2+}$*/$\{[Ru(bpy)_3]^{2+}\cdots[S_2O_8]^{2-}$ that converts to the lower-lying **TA2/T2** state via spin−orbit interaction. Thus, the **TA2/T2** state is most likely involved in the photodissociation at the early stages, serving as an intermediate in the **SA1/S1** → **TA2/T2** → **TA1/T1** chain, where the second step is the highly efficient (spin-allowed) internal conversion. Once the system has converted to **TA1/T1**, it can evolve toward charge transfer from $[Ru(bpy)_3]^{2+}$* to $[S_2O_8]^{2-}$ to form $[Ru(bpy)_3]^{3+}$, SO_4^{2-}, and SO_4^- via elongation of the peroxo O−O bond that brings the zero-order states of the $[Ru(bpy)_3]^{2+}$* and $[S_2O_8]^{2-}$ fragments into (near) resonance.

Steady-state luminescence studies of the quenching of $[Ru(bpy)_3]^{2+}$* in aqueous solutions by $[S_2O_8]^{2-}$ at pH 7.2 and 20 mM sodium phosphate buffer, the exact conditions used in our previous paper,[3] show that 61% of $[Ru(bpy)_3]^{2+}$ form a ground-state ion-pair complex $[Ru(bpy)_3]^{2+}\cdots[S_2O_8]^{2-}$, and the unimolecular ET rate is 2.5 times faster than that of the bimolecular process. The concentration of the ion-pair complexes decreases at higher sodium phosphate buffer.

An exciton interaction model in combination with a transition charge density model, employed here for quantitative analysis of electronic states, is shown to provide an excellent agreement with TD-DFT for the first few excited states of the $[Ru(bpy)_3]^{2+}\cdots[S_2O_8]^{2-}$ complex and allows us to garner insight into electron transfer process. Since this is a facile approach for elucidating the nature of electronic wave functions and understanding their role in energy transfer dynamics and is less time-consuming, the approach looks very promising for applications to large systems.

Acknowledgment. The present research is supported in part by Grant DE-FG02-07ER15906 of the U.S. Department of Energy. The use of computational resources at the Cherry Emerson Center for Scientific Computation is also acknowledged.

Supporting Information Available: Complete references 26 and 28 and Table S1. Cartesian coordinates (in Å) of all structures discussed in the paper. This information is available free of charge via the Internet at http://pubs.acs.org.

References and Notes

(1) Geletii, Y. V.; Botar, B.; Kögerler, P.; Hillesheim, D. A.; Musaev, D. G.; Hill, C. L. *Angew. Chem., Int. Ed.* **2008**, *47*, 3896–3899.
(2) Sartorel, A.; Carraro, M.; Scorrano, G.; Zorzi, R. D.; Geremia, S.; McDaniel, N. D.; Bernhard, S.; Bonchio, M. *J. Am. Chem. Soc.* **2008**, *130*, 5006–5007.
(3) Geletii, Y. V.; Huang, Z. Q.; Hou, Y.; Musaev, D. G.; Lian, T. Q.; Hill, C. L. *J. Am. Chem. Soc.* **2009**, *131*, 7522–7523.
(4) (a) Bard, A. J.; Fox, M. A. *Acc. Chem. Res.* **1995**, *28*, 141–145. (b) White, H. S.; Becker, W. G.; Bard, A. J. *J. Phys. Chem.* **1984**, *88*, 1840.
(5) Kalyanasundaram, K. *Coord. Chem. Rev.* **1982**, *46*, 159–244.
(6) Caspar, J. V.; Meyer, T. J. *J. Am. Chem. Soc.* **1983**, *105*, 5583–5590.
(7) Ferraudi, G.; Arguello, G. A. *Inorg. Chim. Acta* **1988**, *144*, 53–55.
(8) Hauser, A.; Kraussz, E. *Chem. Phys. Lett.* **1987**, *138*, 355–360.
(9) Henbest, K.; Douglas, P.; Garley, M. S.; Mills, A. *J. Photochem. Photobiol. A: Chem.* **1994**, *80*, 299–305.
(10) Damrauer, N. H.; Cerullo, G.; Yeh, A.; Boussie, T. R.; Shank, C. V.; McCusker, J. K. *Science* **1997**, *275*, 54–5.
(11) Damrauer, N. H.; Weldon, B. T.; McCusker, J. K. *J. Phys. Chem. A* **1998**, *102*, 3382–3397.
(12) Yeh, A.; Shank, C. V.; McCusker, J. K. *Science* **2000**, *289*, 935–938.
(13) Zheng, K.; Wang, J.; Shen, Y.; Kuang, D.; Yun, F. *J. Phys. Chem. A* **2001**, *105*, 7248–7253.
(14) Bhasikuttan, A. C.; Suzuki, M.; Nakashima, S.; Okada, T. *J. Am. Chem. Soc.* **2002**, *124*, 8398–8405.
(15) McCusker, J. K. *Acc. Chem. Res.* **2003**, *36*, 876–887.
(16) Anderson, N. A.; Lian, T. *Coord. Chem. Rev.* **2004**, *248*, 1231–1246.
(17) Tarnovsky, A. N.; Gawelda, W.; Johnson, M.; Bressler, C.; Chergui, M. *J. Phys. Chem. B* **2006**, *110*, 26497–26505.
(18) Dietzek, B.; Kiefer, W.; Blumhoff, J.; Botcher, L.; Rau, S.; Walther, D.; Uhlemann, U.; Schmitt, M.; Popp, J. *Chem.—Eur. J.* **2006**, *12*, 5105–5115.
(19) Chang, C.-W.; Chou, C. K.; Chang, I.-J.; Lee, Y.-P.; Diau, E. W.-G. *J. Phys. Chem. C* **2007**, *111*, 13288–13296.
(20) Youngblood, W. J.; Lee, S.-H. A.; Kobayashi, Y.; Hernandez-Pagan, E. A.; Hoertz, P. G.; Moore, T. A.; Moore, A. L.; Gust, D.; Mallouk, T. E. *J. Am. Chem. Soc.* **2009**, *131*, 926–92.
(21) Scholes, G. D. In *Resonance Energy Transfer*; Wiley: New York, 1998.
(22) Howard, I. A.; Zutterman, F.; Deroover, G.; Lamoen, D.; Van Alsenoy, C. *J. Phys. Chem. B* **2004**, *108*, 19155–19162.
(23) (a) Becke, A. D. *J. Chem. Phys.* **1993**, *98*, 1372–1380. (b) Lee, C.; Yang, W.; Parr, R. G. *Phys. Rev. B.* **1998**, *37*, 785–78.
(24) (a) Hay, P. J.; Wadt, W. R. *J. Chem. Phys.* **1985**, *82*, 270–283. (b) Wadt, W. R.; Hay, P. J. *J. Chem. Phys.* **1985**, *82*, 284–298. (c) Hay, P. J.; Wadt, W. R. *J. Chem. Phys.* **1985**, *82*, 299–310.
(25) (a) Tomasi, J.; Persico, M. *Chem. Rev.* **1994**, *94*, 2027–2094. (b) Cammi, R.; Tomasi, J. *J. Comput. Chem.* **1996**, *16*, 1449–58.
(26) Frisch, M. J. *Gaussian 03*, Revision D.01; Gaussian, Inc.: Wallingford, CT, 2004.
(27) Berning, A.; Schweizer, M.; Werner, H.-J.; Knowles, P. J.; Palmieri, P. *Mol. Phys.* **2000**, *98*, 1823–1833.
(28) Werner, H.-J.; Knowles, P. J.; MOLPRO, version 2008.1, a package of *ab initio* programs; see http://www.molpro.net.
(29) Mulliken, R. S. *J. Chem. Phys.* **1955**, *23*, 1833–1837.
(30) McKee, M. L. *J. Phys. Chem.* **1996**, *100*, 3473–3481.

JP908409N